Flight Control Study of an Virtual Insect by a Simulation*

Futoshi TANAKA**, Toshiatsu OHMI***,
Shigeaki KURODA*** and Kazuhiro HIRASAWA****

In this paper, we show an approach to elucidate the free flight of an insect using a simulation. We modeled a fly, Drosophila, by using aerodynamics, body dynamics, and control theory. The modeled virtual insect performs free flight in virtual space generated by a computer. We simulated the free flight of a virtual insect having two dimensions and two degrees of freedom. The flight pass and flight velocity of the virtual insect during a free flight were calculated by Newton's equations of motion. The aerodynamic force generated by the flapping motion of the virtual insect was estimated by using the blade element theory. An optimal regulator theory was used as a control law. The flight pass from the initial position to the target position and the wing motion was obtained from the results of the free flight simulation of the virtual insect. We can presume the wing motion of an insect in free flight by using the flight simulation of a virtual insect. These results have suggested that the approach based on the simulation is effective in elucidating the free flight of an insect.

Key Words: Biomechanics, Modeling, Flight Control, Virtual Insect, Simulation, Free Flight, Optimal Regulator Theory

1. Introduction

Present flying insects have survived the process of natural selection for a long time and have significantly evolved. The flight performances of insects are acrobatic to the extent that they turn on a pinpoint, fly sideways, and even sit upside down on a ceiling. These flight performances are of great interest to us.

Researches based on observation have been conducted to elucidate the free flight of an insect about generation mechanisms of the high forces produced by flapping wings[1]-[4]. For example, delayed stall, rotational circulation, and wake capture were pointed out as generation mechanisms of insect's unsteady fluid force recently[5]. However, the experimental researches of the past have been primarily conducted on a tethered insect. The researches of free flight of the insects are very little[6],[7]. It is because it is very difficult to evaluate the behavior of an insect during free flight.

In this paper, an approach using simulation was attempted to elucidate the free flight of an insect. Purpose of this research is to analyze the motion of a pair of wings of an insect and the flight pass during free flight by using simulation of a modeled insect. We treated free flight of the insect with two dimensions and two degrees of freedom for the simplification. The flapping of a pair of wings is controlled based on the optimal regulator theory, and the aerodynamic force generated by a pair of wings of an insect is calculated by the blade element theory. We simulated the free flight of a fly, Drosophila, with two dimensions and two degrees of freedom from an initial position to a target position. During the free flight, the motion of a pair of wings of an insect and the flight pass were analyzed.

2. Principles

The view in the lateral direction and vertical direction to a stroke plane of an insect are shown in Fig. 1. $\theta(t)$ is the stroke angle between the stroke plane and x axis, as shown in Fig. 1 (a). $\phi(t)$ is the flapping amplitude based on the lateral axis, as shown in Fig. 1 (b). The beating motion of an insect comprises flapping and feathering motion.

The flapping and feathering motion of an insect are

* Received 15th June, 2005 (No. 05-4077)

** Department of Mechanical and Intellectual Systems Engineering, Toyama University, 3190 Gofuku, Toyama-shi, Toyama 930–8555, Japan.
E-mail: f-tanaka@eng.u-toyama.ac.jp

*** Department of Mechanical Engineering and Intelligent Systems, The University of Electro-Communications, 1–5–1 Chofugaoka, Chofu-shi, Tokyo 182–8585, Japan

**** Fluid Technology Ltd., 1–43–3–205 Fuda, Chofu-shi, Tokyo 182–0024, Japan

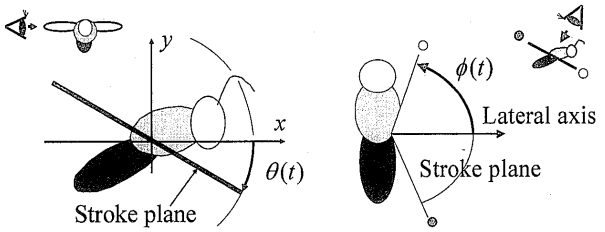

(a) Stroke angle $\theta(t)$ (b) Flapping amplitude $\phi(t)$

Fig. 1 The lateral view and the view from the vertical direction to the stroke plane

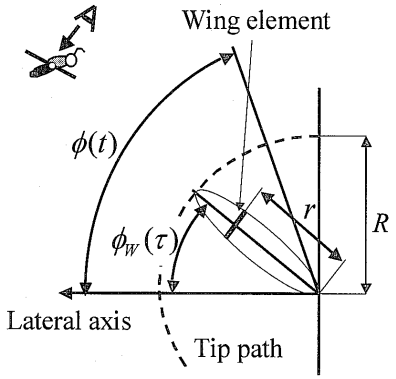

Fig. 2 Flapping motion of a wing

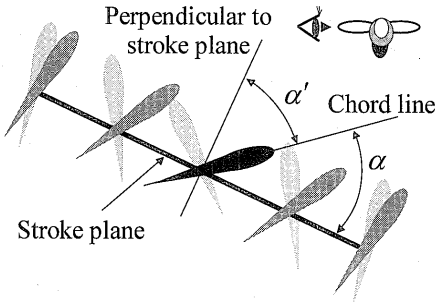

Fig. 3 Feathering motion of a wing

shown in Figs. 2 and 3, respectively. The flapping motion is the rotation around the vertical axis to the stroke plane, as shown in Fig. 2. The feathering motion is the rotation of the angle of attack, as shown in Fig. 3. $\alpha(\tau)$ is the angle between the stroke plane and wing chord. $\alpha'(\tau)$ is the angle between the perpendicular line to the stroke plane and wing chord.

The flapping and feathering motions are approximated as a trigonometric function as follows:

$$\phi_w(\tau)=\phi(t)\sin(2\pi f\tau), \tag{1}$$

$$\alpha(\tau)=\alpha'(\tau)+\frac{\pi}{2}, \tag{2}$$

$$\alpha'(\tau)=\alpha_0\cos(2\pi f\tau), \tag{3}$$

$$0\le\tau\le\frac{1}{f}, \tag{4}$$

where τ is the time during a cycle of flapping motion. f is the beating frequency. $\phi(t)$ is changed in every cycle of the flapping motion. $\phi_w(\tau)$ is the wing position during a cycle of flapping motion. α_0 is the feathering amplitude. t is the time during free flight.

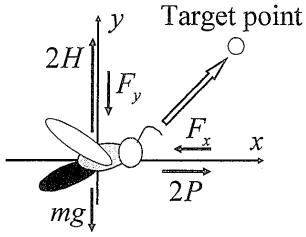

Fig. 4 Schematic representation of an insect

2.1 Equations of motion

Figure 4 shows the schematic of an insect during free flight. In this paper, we simulated the free flight of insect in stationary air. A flight pass of the insect is fixed to a two-dimensional plane, and it is assumed that insects move only in the vertical and horizontal directions.

The equations of motion, which determine the position and velocity of an insect, are as follows:

$$m\ddot{y}=-mg+2H-F_y, \tag{5}$$

$$m\ddot{x}=2P-F_x, \tag{6}$$

where m is the mass of an insect and P and H are the average aerodynamic forces, which are generated by each wing in the x and y directions in a stroke. F_x and F_y are the aerodynamic drag acting on the body of an insect in the x and y directions. g is acceleration due to gravity.

2.2 Aerodynamic force

We estimated the aerodynamic force generated by the wings of an insect on the basis of the blade element theory proposed by Walker[8]. This method decomposes the aerodynamic force into the components of the dynamic pressure and added mass.

$$P=P_d+P_a \tag{7}$$

$$H=H_d+H_a \tag{8}$$

where P_d and H_d are the dynamic pressure force components, P_a and H_a are the added mass force components.

First, the wings are divided in the span wise direction, r; and then, each component of the aerodynamic force acting on each blade element is calculated; finally, the aerodynamic force acting on each blade element is integrated in the span wise direction, r.

2.2.1 Dynamic pressure force Figure 5 shows the component of the velocity depending on the feathering motion. $x_rc(r)$ and $x_ic(r)$ are the distances from the leading edge to the feathering axis and from the leading edge to the action point on the blade element, respectively. x_r and x_i are supplied by the experimental data. We used 0.25 and 0.75, which is used by Walker[8], as the values of x_r and x_i, respectively.

$V_t(r,\tau)$ and $V_r(r,\tau)$, shown in Fig. 5, are the velocities that depend on the flapping and feathering motions, respectively.

$$V_t(r,\tau) = r\dot{\phi}_w(\tau), \tag{9}$$

$$V_r(r,\tau) = (x_i - x_r)c(r)\dot{\alpha}(t). \tag{10}$$

$V(r,\tau)$ shown in Fig. 6 is composed of $V_t(r,\tau)$, $V_r(r,\tau)$, and the moving velocity of the insect. α_{RE} is the angle between the stroke plane and direction of $V(r,\tau)$. $V(r,\tau)$ and α_{RE} are given as follows:

$$V(r,\tau) = \sqrt{(V_t(r,\tau) + V_r(r,\tau)\cos(\alpha') + \dot{x}\cos\theta(t) - \dot{y}\sin\theta(t))^2 + (V_r(r,\tau)\sin(\alpha') - \dot{x}\sin\theta(t) - \dot{y}\cos\theta(t))^2}, \tag{11}$$

$$\alpha_{RE} = \mathrm{Tan}^{-1}\frac{V_r(r,\tau)\sin(\alpha') - \dot{x}\sin\theta(t) - \dot{y}\cos\theta(t)}{V_t(r,\tau) + V_r(r,\tau)\cos(\alpha') + \dot{x}\cos\theta(t) - \dot{y}\sin\theta(t)}, \tag{12}$$

The effective angle of attack is composed of α and α_{RE}.

The lift dL and drag force dD are generated on the blade element in the directions that are both vertical and horizontal directions to $V(r,\tau)$. The lift dL and drag force dD, while depending on the dynamic pressure acting on each blade element, are given as follows:

$$dL = \frac{1}{2}\rho c(r) V(r,\tau)^2 C_L dr, \tag{13}$$

$$dD = \frac{1}{2}\rho c(r) V(r,\tau)^2 C_D dr, \tag{14}$$

where ρ is the density of air, $c(r)$ is the wing chord, $V(r,\tau)$ is the resultant velocity acting on the blade element, and C_L and C_D are the lift and drag coefficients, respectively. C_L and C_D are the empirically derived lift and drag coefficients measured from oscillating wings[5]. C_L and C_D are given as follows:

$$C_L = 0.225 + 1.58\sin(2.13(\alpha + \alpha_{RE}) - 7.2), \tag{15}$$

$$C_D = 1.92 - 1.55\cos(2.04(\alpha + \alpha_{RE}) - 9.82). \tag{16}$$

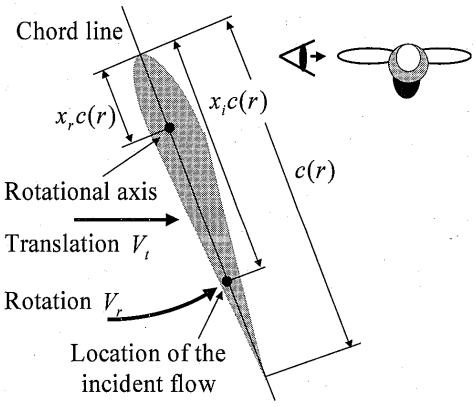

Fig. 5 The velocity depending on the feathering motion

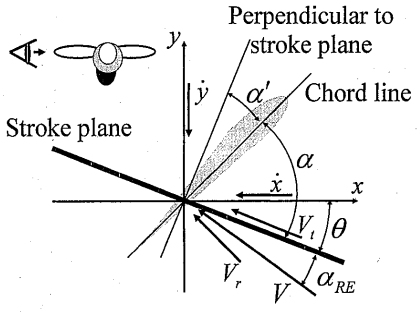

Fig. 6 Air speed acting on the blade element

dL and dD, estimated from Eqs. (13) and (14), act on the blade element in directions that are vertical and horizontal to the resultant velocity. Therefore, dP_d and dH_d, which are the components of the dynamic pressure of the aerodynamic force in the x and y directions, are given as follows:

$$dP_d = dL\sin(\theta + \alpha_{RE}) - dD\cos(\theta + \alpha_{RE}), \tag{17}$$

$$dH_d = dL\cos(\theta + \alpha_{RE}) + dD\sin(\theta + \alpha_{RE}). \tag{18}$$

The total dynamic pressure force acting on the wing is obtained by integrating dP_d and dH_d in the span wise direction.

$$P_d = \int_0^R dP_d \tag{19}$$

$$H_d = \int_0^R dH_d \tag{20}$$

2.2.2 Added mass force The added mass force that vertically acts on the blade element is given as follows:

$$F_a = \int_0^R \frac{\pi}{4}\rho c(r)^2 \dot{v}_n \beta_n dr, \tag{21}$$

$$\dot{v}_n = r\ddot{\phi}_w\cos a' + (\ddot{x}_i - \ddot{x}_r)c(r)\ddot{\alpha} + \ddot{x}\cos\theta\cos a' - \ddot{y}\sin\theta\cos a', \tag{22}$$

where $\dot{v}_n$ is the acceleration in the vertical direction to the wing chord and β_n is the added mass coefficient of the wing section. We used 1.0, which is used by Walker[8]. The added mass force is decomposed into P_a and H_a, as shown in Fig. 7.

$$P_a = -F_a\cos(\theta + \alpha') \tag{23}$$

$$H_a = F_a\sin(\theta + \alpha') \tag{24}$$

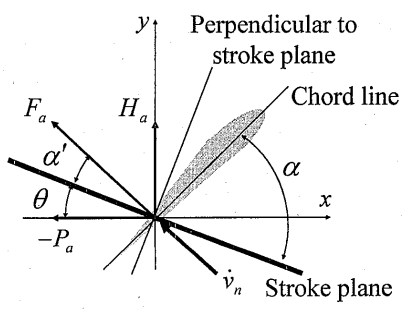

Fig. 7 Distribution of the added mass around the blade element

2.3 Aerodynamic drag acting on the body of the virtual insect

The aerodynamic drag acting on the body of the virtual insect is given as follows:

$$F_x = \frac{1}{2}\rho S\,(\dot{x}^2+\dot{y}^2)\,C_f \cos\beta, \tag{25}$$

$$F_y = \frac{1}{2}\rho S\,(\dot{x}^2+\dot{y}^2)\,C_f \sin\beta, \tag{26}$$

where $\beta = \mathrm{Tan}^{-1}\dfrac{\dot{y}}{\dot{x}}$, $S = \pi R^2$.

The body of the virtual insect was assumed to be a sphere, and its radius is assumed to be the wingspan of the virtual insect. An aerodynamic drag coefficient $C_f = 1.0$ was used.

2.4 Control law

The virtual insect controls the stroke angle $\theta(t)$ and the flapping amplitude $\phi(t)$ required for achieving flight control. The stroke angle and flapping amplitude modulate the direction and magnitude of the aerodynamic force, respectively. In order to transform the equations of motion, the stroke angle and flapping amplitude are represented as the sum of the equilibrium value, $\bar{\theta}$, $\bar{\phi}$, and the fluctuation, $\tilde{\theta}$, $\tilde{\phi}$, from the equilibrium value, respectively.

$$\theta = \bar{\theta} + \tilde{\theta} \tag{27}$$

$$\phi = \bar{\phi} + \tilde{\phi} \tag{28}$$

Equations (5) and (6) are transformed into linear equations. Based on the result of linearization, the controlled systems are expressed as follows:

$$\dot{X} = AX + BU, \tag{29}$$

$$Y = CX, \tag{30}$$

$$X = (x_1, x_2, x_3, x_4)^T, \quad U = (u_1, u_2)^T,$$

$$x_1 = y(t) - y_r, \qquad x_2 = \dot{y}(t) = \dot{x}_1,$$

$$x_3 = x(t) - x_r, \qquad x_4 = \dot{x}(t) = \dot{x}_3,$$

$$u_1 = \tilde{\theta}(t), \qquad u_2 = \tilde{\phi}(t). \tag{31}$$

where X is the state vector, U is the control input, Y is the output vector, and x_r and y_r are the target values. In order to determine the control inputs required to reach the target position, the optimal regulator theory was applied to this linear system. The performance index was applied in a quadratic form as follows:

$$J = \int_0^\infty [X^T Q X + U^T R U]\,dt. \tag{32}$$

The control input U is determined to minimize the performance index. Q and R are the weighting matrix. The weighting matrix Q and R are set as the identity matrix. The optimal state feedback coefficient matrix F is given as follows:

$$F(t) = -R^{-1}B^T P, \tag{33}$$

where P, which is estimated by using the Riccati equation, is a semi-positive definite symmetric matrix. The Riccati equation is given as follows:

$$A^T P + PA + Q - PBR^{-1}B^T P = 0. \tag{34}$$

The state feedback coefficient matrix F is transformed into an optimal control input U by using Eq. (35).

$$U = FX \tag{35}$$

The optimal control inputs are estimated from the linear equations—Eqs. (29) and (30); the input U is used to calculate the new state vector from the non-linear equations—Eqs. (5) and (6).

3. Results and Discussion

Tables 1 and 2 show the calculation condition and the flight parameter, respectively. The flight parameter of a virtual insect was determined by referring to the measurement data of real insects[1),2),9)]. The profile of the wing of the virtual insect was determined by referring to the measurement data of the Drosophila[1)]. The wing was divided into 20 equidistant sections in the spanwise direction.

3.1 Flight control from the initial position to the target position

Figure 8 shows the flight trajectory from the initial position to the target position. The flight trajectory is a straight line.

Figures 9 and 10 show the time histories of the wing motions and the aerodynamic force acting on the wings,

Table 1 Calculation condition

Initial point (x, y) (m)	(0, 0)
Initial velocity (u, v) (m/s)	(0, 0)
Target point (x_r, y_r) (m)	(1.0, 1.0)
Sampling time Δt (s)	4.95×10^{-3}

Table 2 Flight data

Density of air ρ (kg/m^3)	1.184
Beating frequency f (Hz)	202
Wing length R (m)	2.5×10^{-3}
Feathering amplitude α_0 (deg)	55
Mass of an insect m (kg)	2.0×10^{-6}

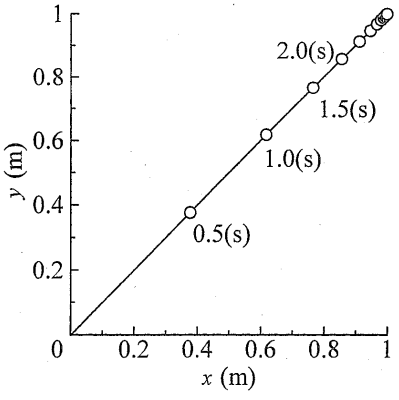

Fig. 8 Flight trajectory from the initial position to the target position

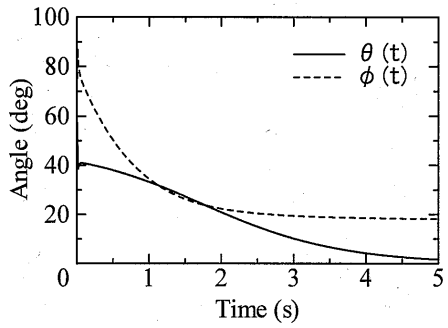

Fig. 9 Time histories of the wing motions

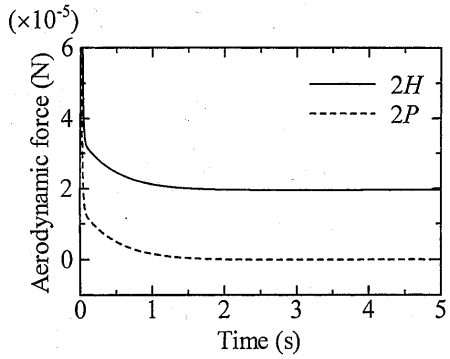

Fig. 10 Time histories of the aerodynamic force in the x and y directions

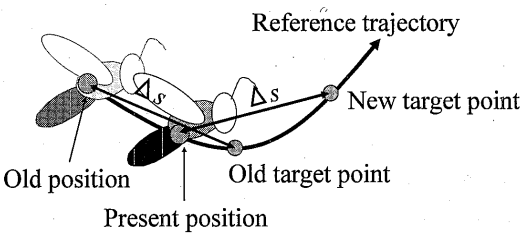

Fig. 11 Schematic model for the tracking of the reference trajectory

respectively. The flapping amplitude ϕ becomes constant after approximately two seconds. However, the curve of the stroke plane angle θ is gradual. The stroke plane angle θ slowly approaches the equilibrium value. On the other hand, as shown by to Fig. 10, both vertical and horizontal aerodynamic forces acting on the wing become constant immediately. A virtual insect approaches the target position by using the air resistance and inertial force that acts on its body. In the vicinity of the target position, the flapping amplitude is approximately 18 degrees, and the angle of the stroke plane is approximately 0 degrees. At this time, the virtual insect simultaneously generates a lift force that balances gravity.

3.2 Tracking the reference trajectory

Figure 11 shows the schematic model of tracking the reference trajectory. In section 3.1, the target position was constant. In this section, the target position is situated at a distance Δs from the present position on the reference trajectory. The target position changes with the passage of time.

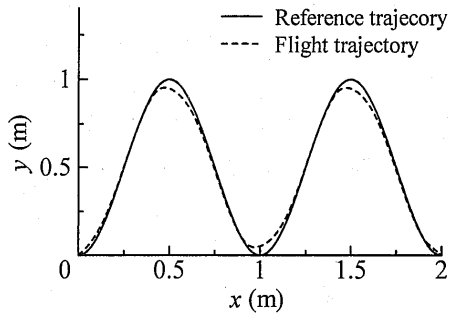

Fig. 12 Flight trajectory for the tracking of the reference trajectory

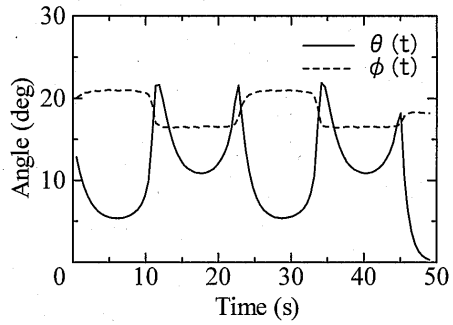

Fig. 13 Time history of the wing motion

The reference trajectory is given as follows:

$$y = 0.5\cos(2\pi x - \pi) + 0.5. \quad (36)$$

Δs of 0.1 m was used.

Figure 12 shows the reference and flight trajectory. The flight trajectory corresponds to the reference trajectory excluding the external point. Figure 13 shows the time history of the wing motion. During a rising flight, the virtual insect generates a lift that is greater than its body weight. As a result, the flapping amplitude of a virtual insect increases more than that during the hovering flight. In descending flight, the flapping amplitude of a virtual insect decreases more than that during the hovering flight. The virtual insect descends due to gravity. The fluctuation of the stroke angle is larger than that of the flapping amplitude. A virtual insect is primarily controlled by the angle of the stroke plane. The virtual insect tracked the reference trajectory by using the simple control law. We can presume the wing motion of an insect in free flight by using the flight simulation of a virtual insect.

4. Conclusion

From the free flight simulation of the virtual insect, we concluded the following.

(1) The free flight of the virtual insect with two dimensions and two degrees of freedom can be controlled by using the simple control law that used the optimal regulator theory.

(2) The flight pass from the initial position to the tar-

get position and wing motion was obtained by the results of the free flight simulation of the virtual insect.

(3) We can presume the wing motion of an insect in free flight by using the flight simulation of a virtual insect.

These results have suggested that the approach based on the simulation is effective in elucidating the free flight of an insect.

References

(1) Weis-Fogh, T., Energetics of Hovering Flight in Hummingbirds and in Drosophila, J. Exp. Biol., Vol.56 (1972), pp.79–104.

(2) Weis-Fogh, T., Quick Estimates of Flight Fitness in Hovering Animals, Including Novel Mechanism for Lift Production, J. Exp. Biol., Vol.59 (1973), pp.169–230.

(3) Ellington, C.P., The Aerodynamics of Hovering Insect Flight I-VI, Phil. Trans. R. Soc. Lond. B., Vol.305 (1984), pp.1–181.

(4) Azuma, A. and Watanabe, T., Flight Performance of a Dragonfly, J. Exp. Biol., Vol.137 (1988), pp.221–252.

(5) Dickinson, M.H., Lehmann, F. and Sane, S.P., Wing Rotation and the Aerodynamic Basis of Insect Flight, Science, Vol.284 (1999), pp.1954–1960.

(6) Dudley, R. and Ellington, C.P., Mechanics of Forward Flight in Bumblebees I. Kinematics and Morphology, J. Exp. Biol., Vol.148 (1990), pp.19–52.

(7) Dudley, R. and Ellington, C.P., Mechanics of Forward Flight in Bumblebees II. Quasi-Steady Lift and Power Requirements, J. Exp. Biol., Vol.148 (1990), pp.53–88.

(8) Walker, J.A., Rotational Lift: Something Different or More of the Same?, J. Exp. Biol., Vol.205 (2002), pp.3783–3792.

(9) Zanker, J.M. and Gotz, K.G., The Wing Beat of Drosophila Melanogaster I-II, Phil. Trans. R. Soc. Lond. B., Vol.327 (1990), pp.1–44.